Acta Metall. Sin. (Engl. Lett.), 2018, **31**, 371–379
https://doi.org/10.1007/s40195-017-0621-4

Crystallographic Texture Evolution of γ′-Fe_4N and Its Influences on Tribological Property of Nitrided Steel

Yi-Xue Wang[1,2] · Mu-Fu Yan[1] · Zhao-Bo Chen[2] · Cheng-Song Zhang[3] · Yuan You[2,4]

Received: 25 April 2017 / Revised: 2 June 2017 / Published online: 12 July 2017

Abstract The crystallographic texture of γ′-Fe_4N in compound layer and its influences on the tribological properties of nitrided steel 38CrMoAl are investigated in the study. The preferred orientation of $(200)\gamma'$ is produced by low-temperature nitriding in atmosphere with low nitrogen–hydrogen ratio and increases with the nitriding time. The preferred orientation of $(220)\gamma'$ appears after 72 h cyclic nitriding. The orientation relationships $(0001)_\varepsilon//(101)_{\alpha'}$ and $[110]_\varepsilon//[111]_{\alpha'}$, $(111)_{\gamma'}//(0001)_\varepsilon$ and $[011]_{\gamma'}//\left[1\bar{2}10\right]_\varepsilon$, $(200)_{\gamma'}//(110)_{\alpha'}$ and $[011]_{\gamma'}//[111]_{\alpha'}$, as well as $\left(1\bar{1}03\right)_\varepsilon//(220)_{\gamma'}$ and $[0100]_\varepsilon//\left[1\bar{1}0\right]_{\gamma'}$ are established by first-principles method. The misfit of interatomic distance (δ), determining the phase transition resistance, is calculated. Accordingly, two reaction pathways during nitriding, $\alpha'\rightarrow\gamma'$ and $\alpha'\rightarrow\varepsilon\rightarrow\gamma'$, are assumed, which determines the preferred orientations of γ′-Fe_4N. Results of wear tests demonstrate that the specimen with preferred orientation of $(200)\gamma'$ exhibits lower frictional coefficient and lower wear rate in comparison with the specimen with $(220)\gamma'$ preferred orientation. $(111)\gamma'$ texture usually relates to the lower frictional coefficient but higher wear rate due to the main slip system parallel to the sliding plane. Therefore, the $(200)\gamma'$ preferred orientation has a positive significance in improving the wear properties of steels.

KEY WORDS: Crystallographic orientation; First-principles calculation; Plasma nitriding; Tribological property

1 Introduction

Crystallographic orientation is always known as one of the main factors affecting the obdurability of metallic materials for structural applications. Generally speaking, the failure of metallic materials, especially the steels and the stainless steels, usually occurs in the surface layer. For instance, the wear and fatigue always initiated by tiny cracks on the surface or in the subsurface layer of workpieces, which is directly related to slip band emergence [1, 2]. The crystallographic texture in the surface layer always influences the tribological and fatigue properties to a large extent [3–11]. A drop in the frictional coefficient with progressive texture can be found as a result of easy glide planes parallel to the sliding plane [3]. The texture is shown to affect the stress–strain response of the material and the fatigue

Available online at http://link.springer.com/journal/40195

✉ Mu-Fu Yan
yanmufu@hit.edu.cn; prsm804@163.com

[1] National Key Laboratory for Precision Hot Processing of Metals, School of Materials Science and Engineering, Harbin Institute of Technology, Harbin 150001, China

[2] School of Mechatronics Engineering, Harbin Institute of Technology, Harbin 150001, China

[3] School of Materials Science and Engineering, Southwest Jiaotong University, Chengdu 610031, China

[4] School of Materials Science and Engineering, Qiqihar University, Qiqihar 161006, China

damage (crack density) according to the research of Mineur [4]. Bertolino et al. [5] reveal that a large scatter in transgranular crack growth rates is related to the local textures, which essentially influence the endurance limit. Recent studies indicate that the progressive preferred orientation is essential for the performance and lifetime of steel components and can be obtained by surface treatments [6, 12–14], such as coating [13], thermochemical treatments and laser methods [14]. Plasma nitriding is an effective thermochemical treatment, and the change in crystallographic texture after plasma nitriding of austenite stainless steel has been already reported [12]. Moreover, the lattice rotation of several degrees has been found by Abrasonis et al. [15], suggesting that the crystallographic texture in the nitrided layer of austenite stainless steel can be controlled by adjusting the experimental parameters during plasma nitriding. Stinville et al. [12] interpret that the lattice rotation and the direction of rotation are directly related to the initial orientation at the surface of the original material.

Till now, most studies about the crystallographic texture produced by plasma nitriding are limited on the austenite stainless steel rather than martensitic steel. Plasma nitriding of martensitic steels performed at a conventional temperature around 550 °C produces several microns thick compound layer followed by a diffusion region [16]. The phases within the nitrided layer are usually composed of iron nitrides (ε-$Fe_{2-3}N$ with trace of γ′-Fe_4N phases) for low-alloy steels. Recent studies [17–19] on low-temperature nitriding demonstrate that the nitrided layer is composed mainly of γ′ phase with significant preferred orientation of (200)γ′, if the plasma nitriding is conducted below 460 °C with low nitrogen supply. Such layer is found to be further optimized with the increased hardness, the reduced wear rate and the improved corrosion resistance. However, the correlation between the crystallographic texture of γ′ and the mechanical properties has not been clarified yet. It is predicted that the phase composition of reaction product is close related to the nitriding temperature and the concentration of nitrogen. And the crystallographic texture of (200)γ′ is related to the orientation relationship between the nitrides and matrix.

The aim of the present work is to investigate the crystallographic texture of γ′ produced by plasma nitriding through first-principles method and study its effects on tribological properties of nitrided steels.

2 Materials and Methods

The 38CrMoAl steel with composition of (wt.%) 0.4 C, 0.2 Si, 0.81 Mn, 1.52 Cr, 1.08 Al, 0.22 Mo and balance Fe is used. Before plasma nitriding, the steel is solution treated at 940 °C for 1 h and then quenched in oil. After that, the steel specimens are machined into ϕ25 mm × 5 mm round disks. Then the flat faces of the specimens are manually ground down to 800 grades by silicon carbide papers to achieve a fine finish. The specimens are ultrasonically rinsed thoroughly with distilled water, alcohol and acetone before plasma treatment.

Plasma nitriding is carried out using a homemade plasma nitriding unit (LDMC-30, 30 kW). Before the application of glow discharge, the chamber is evacuated to 10 Pa by a rotary pump. Plasma nitriding is conducted in a gas mixture of nitrogen and hydrogen (1:8 vol.%) at 460 and 560 °C for 4 h. Conventional plasma nitriding under high nitrogen proportion atmosphere at 560 °C for 4 h in a gas mixture of nitrogen and hydrogen (1:3 vol.%) is conducted simultaneously for comparison. Two series of plasma nitriding, conventional and cyclic, are carried out to clarify the trends of preferred orientation along with the nitriding time at a temperature of 500 °C in a gas mixture of N_2 and H_2 (1:3 vol.%) for 24, 48 and 72 h. After the experiments, the chamber is evacuated and the specimens are left under vacuum to cool down slowly to room temperature.

The phase compositions and the crystallographic information for the untreated and nitrided layers are analyzed using a D/max-rB diffractometer (XRD) with Cu-$K\alpha$ radiation ($\lambda = 0.15405$ nm) in the range of glancing angles 20–100° at 40 kV and 50 mA with 0.05° interval step mode.

The microhardness for the treated surface is measured using a Vickers microhardness tester under a load of 100 g. The tribological properties are evaluated using a reciprocating pin-on-disk tribometer of type POD-1. The nitrided specimens are rotated against a stationary WC ball of 5 mm in diameter under a load of 10 N at a speed of 200 rpm (0.1 m/s) for 3600 s. All tests are conducted in air atmosphere and without lubrication (temperature 21 °C, humidity 43% RH). The wear rate (W_v) is measured to evaluate the wear degree of specimens, which is evaluated by the ratio of volume loss versus sliding distance:

$$W_v = \frac{\Delta V}{LN}, \tag{1}$$

where $\Delta V(\mathrm{mm}^3)$ is volumetric wear loss, N is the normal load (N) and L (m) is the total sliding distance. The volumetric wear loss, $\Delta V(\mathrm{mm}^3)$, is measured according to the procedure given in the ASTM Standard G99, using [20]:

$$\Delta V = 2\pi R\left[\mathrm{r}^2 \sin^{-1}\left(\frac{w}{2r}\right) - \left(\frac{w}{4}\right)\sqrt{4r^2 - w^2}\right], \tag{2}$$

where R and w are the radius and the average width of the wear track, and r is the radius of the counterface ball. The

worn morphologies of the specimens are analyzed using a scanning electron microscope (SEM, FEI Sirion) equipped with an energy-dispersive spectrometer (EDS).

The mechanism for the preferred orientation is elaborated by first-principles method. The calculations in this work are conducted by CASTEP code. Geometry optimizations of the structures are performed within the Broyden–Fletcher–Goldfarb–Shanno (BFGS) minimization scheme, with following thresholds for converged structures: energy change per atom, maximum residual force, maximum atomic displacement, maximum stress less than 5×10^{-6} eV, 0.01 eV/Å, 5×10^{-4} Å and 0.02 GPa, respectively. The exchange correlation potential is treated with generalized gradient approximation (GGA-PBE). In the calculations, the Brillouin zone is sampled with a *k*-point mesh of grid generated by the Monkhorst–Pack method. The cutoff energy (E_{cut}) on the wave function is optimized with lattice parameters and total energy. The checked cutoff energy of 380 eV is used in all the calculations. The valences for the atomic configurations are Fe-$3d^6 4s^2$ and N-$2s^2 2p^3$.

3 Results and Discussion

3.1 Preferred Orientation Characterization

In order to evaluate the γ'-Fe_4N of different preferred orientations in the nitrided layers, three series of experiments are carried out. Figure 1 shows the XRD patterns of the steel 38CrMoAl plasma nitrided under different experimental conditions. Figure 1a shows the phase composition of the specimens nitrided at 460 and 560 °C under atmospheres with different nitrogen–hydrogen ratios. The XRD pattern for the untreated specimen corresponds well to single martensite phase (i.e., α'-Fe). For the specimens treated at 460 °C in the atmosphere of nitrogen and hydrogen (1:8 vol.%), the phase composition is composed of nitrogen expanded martensite (α'_N-Fe) suggested by Kim et al. [21] and γ'-Fe_4N. The preferred orientation of (200)γ' is observed in the nitrided layer, and the tendency reduces with the rising up temperature to 560 °C. For the specimens nitrided at 560 °C with the nitrogen and hydrogen (1:3, vol.%), typical diffraction peaks of γ'-Fe_4N and ε-$Fe_{2-3}N$ can be seen without evident preferred orientation. Thus, the preferred orientation of (200)γ' is obtained under the nitriding condition at low temperature with low nitrogen supply. Figure 1b shows the XRD patterns of steel 38CrMoAl plasma nitrided at 500 °C with the nitrogen and hydrogen (1:3, vol.%) for 24, 48 and 72 h. The phase structure for the nitrided specimens is mainly composed of γ' with a spot of ε and/or α'_N. Increasing preferred orientation of (200)γ' with the nitriding time is presented clearly. However, the preferred orientation strongly depends on the nitriding condition. Figure 1c shows the XRD patterns for the steel 38CrMoAl cyclic plasma nitrided at 420–500 °C with the nitrogen and hydrogen (1:3, vol.%) for 24, 48 and 72 h, in which the preferred orientation of (220)γ' is protruded after 72 h treatment.

The interfacial energy and the elastic strain energy are the main resistances to solid-state transformation. The new phase always precipitates from the parent phase along the habit plane equiaxially and coherently, and therefore, the main resistance of phase transition is the elastic strain energy caused by the misfit of lattice.

3.2 Theoretical Calculation

The first-principles calculation is employed to optimize the lattices of the α'_N, γ'-Fe_4N and ε-$Fe_{2-3}N$, calculate the lattice misfit and evaluate the phase transition. The alloying element M (M = Cr, Mo and Al) occupied the Fe sites according to the chemical composition of the steel 38CrMoAl, and the structures of alloyed γ'-(Fe,M)$_4$N and ε-(Fe,M)$_{2-3}$N and α'-(Fe,M)N_x are built (Fig. 2, the color coding is used to group the correlative planes). These alloyed phases are treated as disordered solid solution in

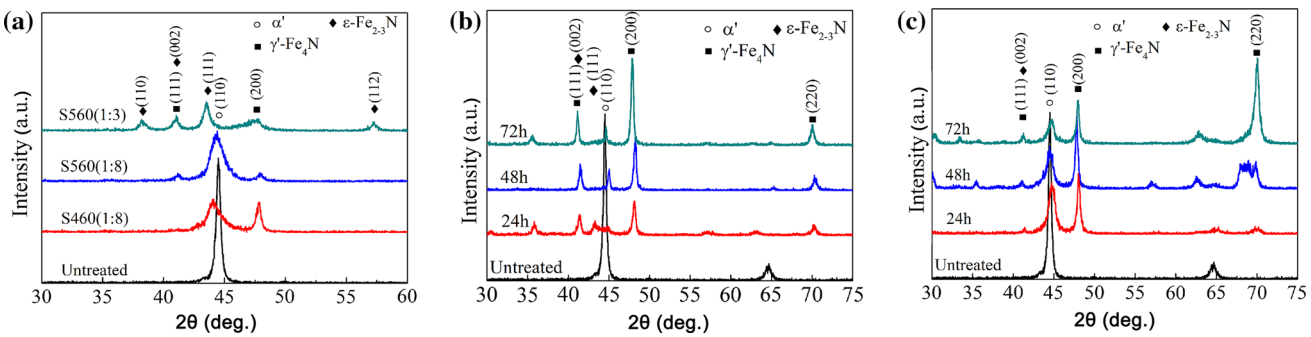

Fig. 1 XRD patterns of nitrided steel 38CrMoAl, **a** plasma nitriding at different temperatures with high/low nitrogen supply, **b** nitriding at 500 °C for different time, **c** cyclic nitriding between 420 and 500 °C for different time

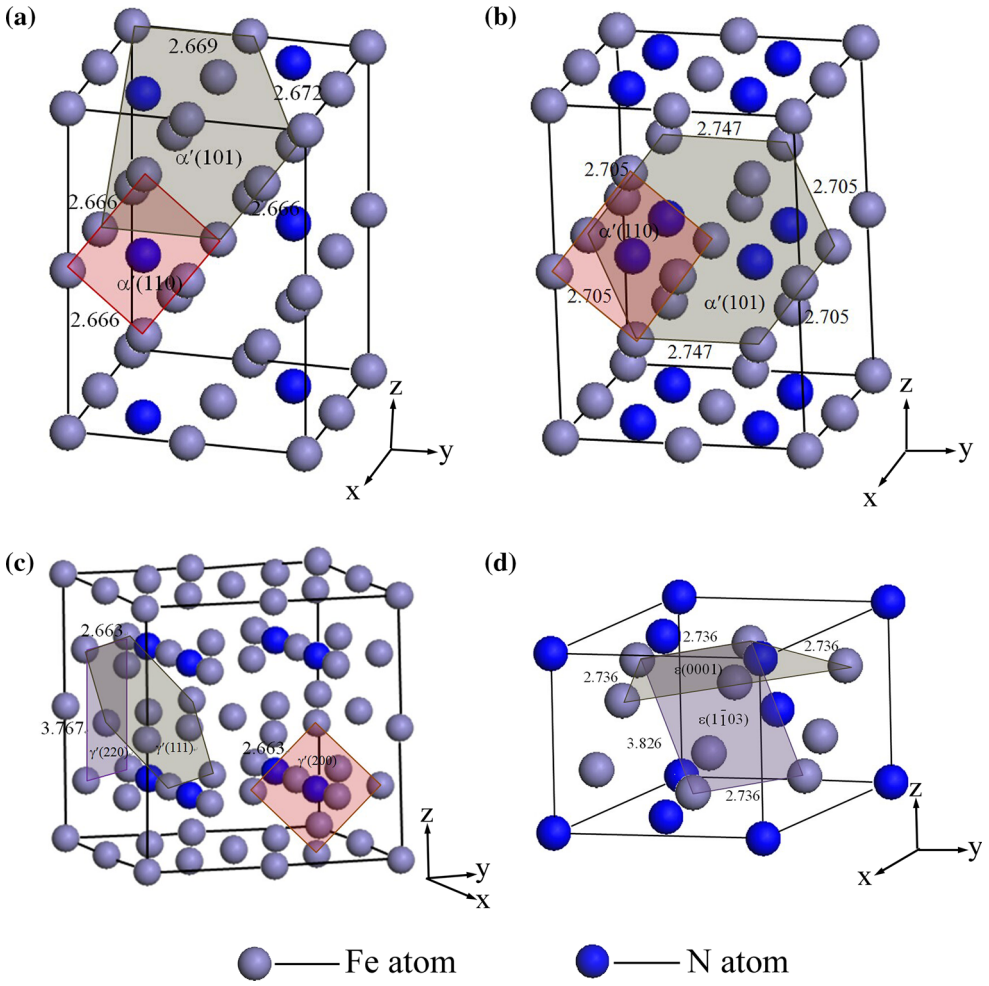

Fig. 2 **a** Crystal structures of α-(Fe,M)$_{(1-x)}$N$_x$ with $x = 0.2$, **b** crystal structures of α-(Fe,M)$_{(1-x)}$N$_x$ with $x = 0.33$, **c** crystal structures of γ′-(Fe,M)$_4$N, **d** crystal structures of ε-(Fe,M)$_{2-3}$N

the VCA framework, considering the atomic sites in terms of a mixture atom. The supercell sizes for α′-(Fe,M)N$_x$ and γ′-(Fe,M)$_4$N are 2 × 2 × 2, containing 16 Fe atoms and 32 Fe atoms, respectively. The ε-(Fe,M)$_{2-3}$N is calculated by single cell.

Figure 2a, b shows the crystal structure of α′-(Fe,M)N$_x$ containing 20 and 33 at.% nitrogen, respectively. Figure 2c, d exhibits the crystal structures of α′-(Fe,M)N$_x$ and ε-(Fe,M)$_{2-3}$N, respectively. The calculated interatomic distances are listed in Table 1.

The misfit of interatomic distance (δ) is utilized to evaluate the matching degree of the lattice.

$$\delta = \frac{\left|D_{\text{precipitate}} - D_{\text{parent}}\right|}{D_{\text{parent}}}, \tag{3}$$

where $D_{\text{precipitate}}$ and D_{parent} represent the interatomic distances of the two phases along the interface, respectively. The larger the δ is, the higher the elastic strain energy is. Coherent relationship remains between the parent phase and precipitates if δ is no more than 5%.

The misfit of interatomic distance (δ) of different crystallographic planes is listed in Table 2. It is clearly that when the nitrogen content of α'_N is up to 20 at.%, the lattice is elongated in the direction of Z axle. The $\{110\}_{\alpha'}$ is found matching to the $\{200\}_{\gamma'}$ and the δ is only 0.11%, while the δ is 2.51% between the planes of $\{101\}_{\alpha'}$ and $\{0001\}_{\varepsilon}$. This demonstrates that the γ′ preferentially precipitates from α'_N under the lower nitrogen proportion condition and maintains the orientation relationship $\{200\}_{\gamma'}//\{110\}_{\alpha'}$ and $[110]_{\gamma'}//[111]_{\alpha'}$ with α'_N; as a result, the preferred orientation of $\{200\}\gamma'$ is remarkable. However, ε preferentially precipitates if the nitrogen content in the lattice of α'_N exceeds 33 at.%, the $\{101\}_{\alpha'}$ matches well to the $\{0001\}_{\varepsilon}$ and the δ decreases from 2.51% to 1.14%. The δ is 2.67% between the planes of $\{111\}_{\gamma'}$ and $\{0001\}_{\varepsilon}$. In this situation, the preferred orientation of $\{200\}\gamma'$ decreases, and the $\{111\}\gamma'$ peaks increase obviously (in Fig. 1). These orientation relationships are also verified by Liu et al. [22]. In the present work, another significant preferred orientation of $\{220\}\gamma'$ is detected for the first

Table 1 Interatomic distances calculated by first-principles calculation

N content	Interatomic distance, D (Å)						
	α'		γ'			ε	
	{110}	{101}	{200}	{111}	{220}	{0001}	$\{1\bar{1}03\}$
$x = 0.2$	2.666	2.669	2.663	2.663	3.767 2.663	–	–
$x = 0.33$	2.705	2.747 2.705	–	–	–	2.736	3.826 2.736

Table 2 Misfit of interatomic distance of different crystallographic planes, δ (%)

N content	$\{110\}\alpha'//\{200\}\gamma'$	$\{101\}\alpha'//\{0001\}\varepsilon$	$\{0001\}\varepsilon//\{111\}\gamma'$	$\{1\bar{1}03\}\varepsilon//\{220\}\gamma'$
$x = 0.2$	0.11	2.51	–	–
$x = 0.33$	1.55	1.14	2.67	2.67 1.54

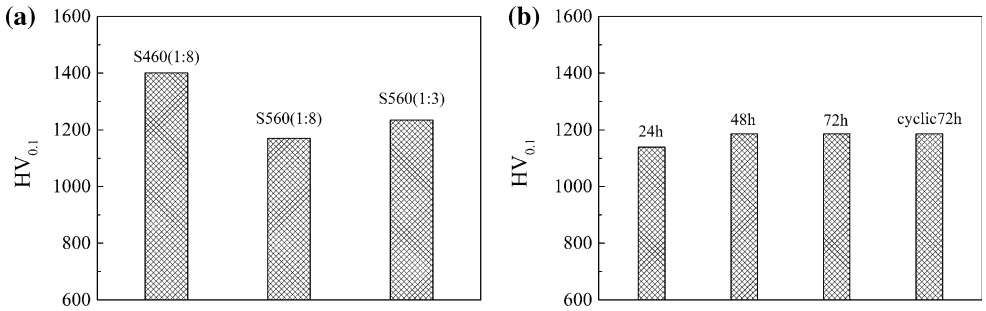

Fig. 3 **a** Microhardness of steel 38CrMoAl surface plasma nitrided at different temperatures with high/low nitrogen supply, **b** microhardness of steel 38CrMoAl plasma nitrided at 500 °C for different time and cyclic nitrided between 420 and 500 °C for 72 h

time during the cyclic plasma nitriding for 72 h. The $\{220\}_{\gamma'}$ is found matching to the $\{1\bar{1}03\}_{\varepsilon}$ and the δ is 1.54 and 2.67% in two directions. That means that the γ' precipitates from ε along the planes of $\{220\}_{\gamma'}//\{1\bar{1}03\}_{\varepsilon}$ gradually due to the lower δ of 1.54% during the vibration of cyclic nitriding. Thus, the preferred orientation of $\{220\}\gamma'$ is protruded spontaneously. However, relative larger δ indicates that the transition of $\varepsilon\rightarrow\gamma'$ always accompanied by denitrification, interatomic distance reduction and lattice distortion.

It is reasonable to assume that two kinds of reaction pathways of the formation of γ'-Fe_4N can be anticipated: $\alpha'\rightarrow\gamma'$ and $\alpha'\rightarrow\varepsilon\rightarrow\gamma'$ (the cyclic nitriding has the same formation). The generated γ'-Fe_4N maintains the coherent relationship with certain planes of α'_N or ε-$Fe_{2-3}N$, so the preferred orientation of γ'-Fe_4N has close relationship with the reaction pathways. The reaction of $\alpha'_N\rightarrow\gamma'$ is dominant during conventional nitriding at lower temperature in the low nitrogen proportion atmosphere with the orientation relationship of $\{200\}_{\gamma'}//\{110\}_{\alpha'}$ and $[011]_{\gamma'}//[111]_{\alpha'}$, resulting in the preferred orientation of $\{200\}\gamma'$. The reaction of $\alpha'_N\rightarrow\varepsilon\rightarrow\gamma'$ will become preferential if the nitriding is conducted at high temperature and/or under the atmosphere with higher nitrogen proportion. Such orientation relationships of $\{0001\}_{\varepsilon}//\{101\}_{\alpha'}$ and $[110]_{\varepsilon}//[111]_{\alpha'}$, $\{111\}_{\gamma'}//\{0001\}_{\varepsilon}$ and $[011]_{\gamma'}//[1\bar{2}10]_{\varepsilon}$ among all the three phases can be established. Thus, the preferred orientation of $\{200\}\gamma'$ will decrease and even vanish. A set of a special orientation relationship of $\{1\bar{1}03\}_{\varepsilon}//\{220\}_{\gamma'}$ and $[0100]_{\varepsilon}//[1\bar{1}0]_{\gamma'}$ is established firstly in the cyclic plasma nitriding experiments, which is the main cause for the preferred orientation of $\{220\}\gamma'$.

Now, how the preferred orientation affects the tribological properties of steels? In the present work, the wear tests and microhardness measurements are performed to characterize the tribological properties of the steel 38CrMoAl with different preferred orientations of γ' on the surface.

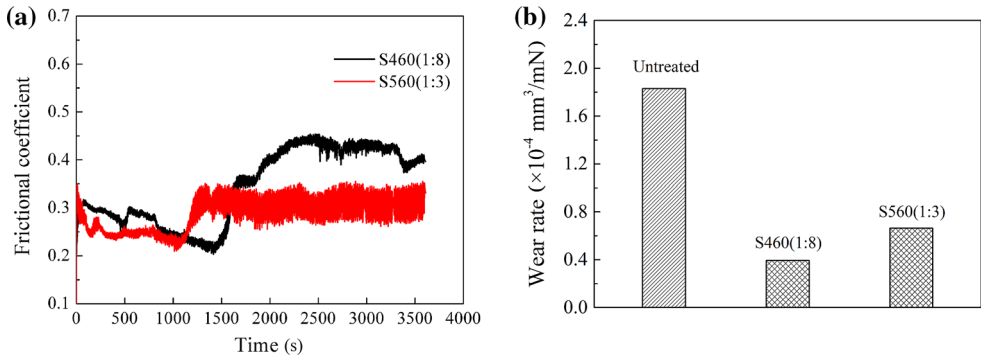

Fig. 4 Frictional coefficients **a** and wear rates **b** of steel 38CrMoAl plasma nitrided at different temperatures with high/low nitrogen supply

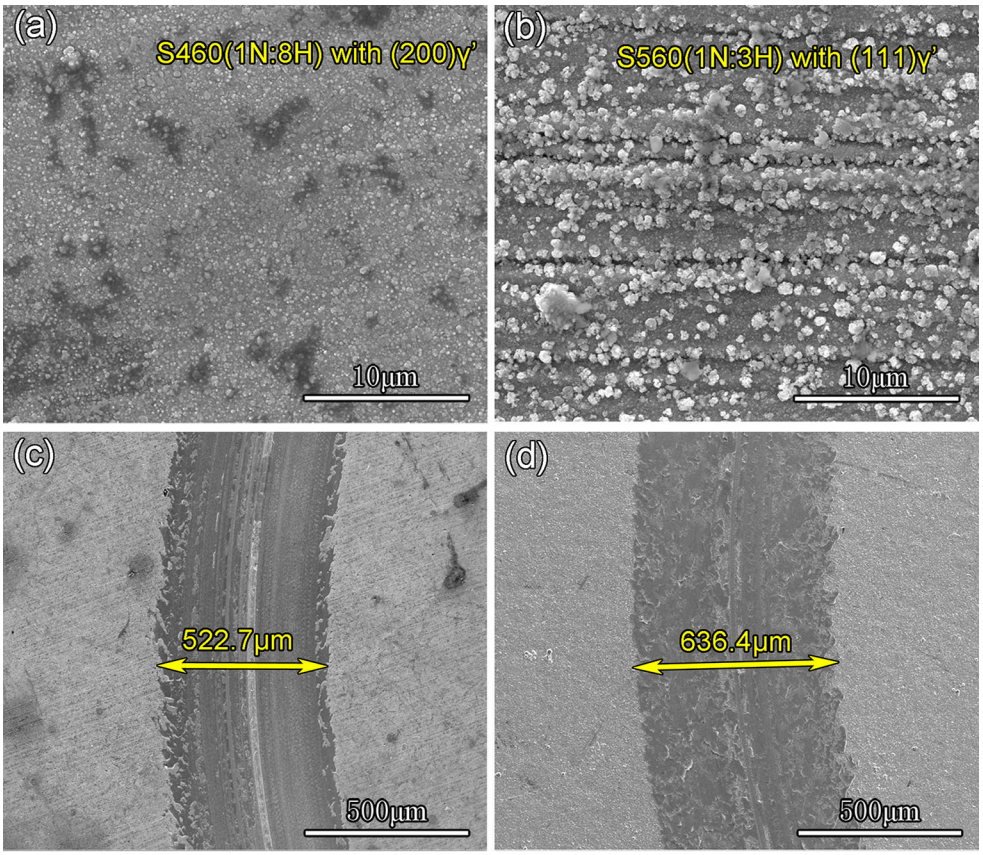

Fig. 5 Surface morphologies and wear tracks of steel 38CrMoAl plasma nitrided at different temperatures with high/low nitrogen supply, **a**, **c** S460(1:8), **b**, **d** S560(1:3)

3.3 Mechanical Properties

3.3.1 Surface Hardness

The surface microhardness for the steel 38CrMoAl of three different γ' preferred orientations is shown in Fig. 3. The S460(1:8) specimen with the phase composition of α'_N and γ' exhibits the highest hardness of 1401 $HV_{0.1}$ in Fig. 3a, which is much higher than that of the S560(1:8) specimen (1170 $HV_{0.1}$). The microhardness of S560(1:3) specimen (1235 $HV_{0.1}$) is a little higher than that of the S560(1:8) counterpart due to the formation of ε phase. Moreover, the surface hardness of the nitrided specimens is almost invariant with the nitriding time, including the cyclic nitriding. Therefore, the different preferred orientations have limited influence on the surface microhardness.

3.3.2 Tribological Properties

Figure 4a shows the frictional coefficients of the steel 38CrMoAl plasma nitrided under different conditions. The S560(1:3) specimen exhibits a much lower frictional coefficient in comparison with the S460(1:8) specimen. For the S560(1:3) specimen, close-packed (111)γ' planes are parallel to the surface, which contributes to the reduction in frictional coefficient as suggested by Zoheir et al. [3]. However, the {111} <110> is the main slip system for FCC structure running easily during sliding. Thus, the lower frictional coefficient and higher wear rate of S560(1:3) specimen compared with the S460(1:8) specimen are observed (see Fig. 4b).

Figure 5 exhibits the surface morphologies and wear tracks for the S560(1:3) and S460(1:8) specimens. The S460(1:8) surface is characterized by much finer particles than the S560(1:3) surface. Consisting with the wear rate measurement, the wear track of S460(1:8) specimen is much narrower and shallower than that of the S560(1:3) specimen. Significant flakes caused by fatigue are observed in the wear track of S560(1:3) specimen (Fig. 5d), demonstrating the occurrence of severe plastic deformation due to running of slip systems. Additionally, the high misfit between the γ' and ε phases, usually meaning high internal stress, is responsible for the severe peeling off during sliding. The preferred orientation of (200)γ' is effective in

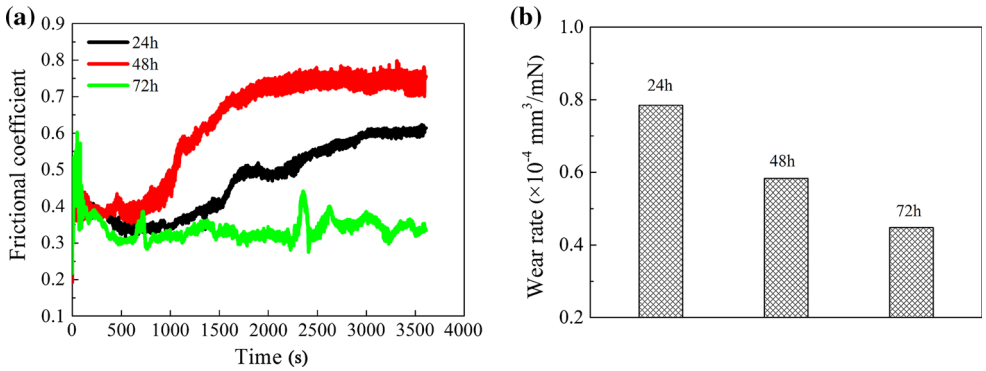

Fig. 6 Frictional coefficients **a** and wear rates **b** of steel 38CrMoAl surfaces plasma nitrided at 500 °C for different time

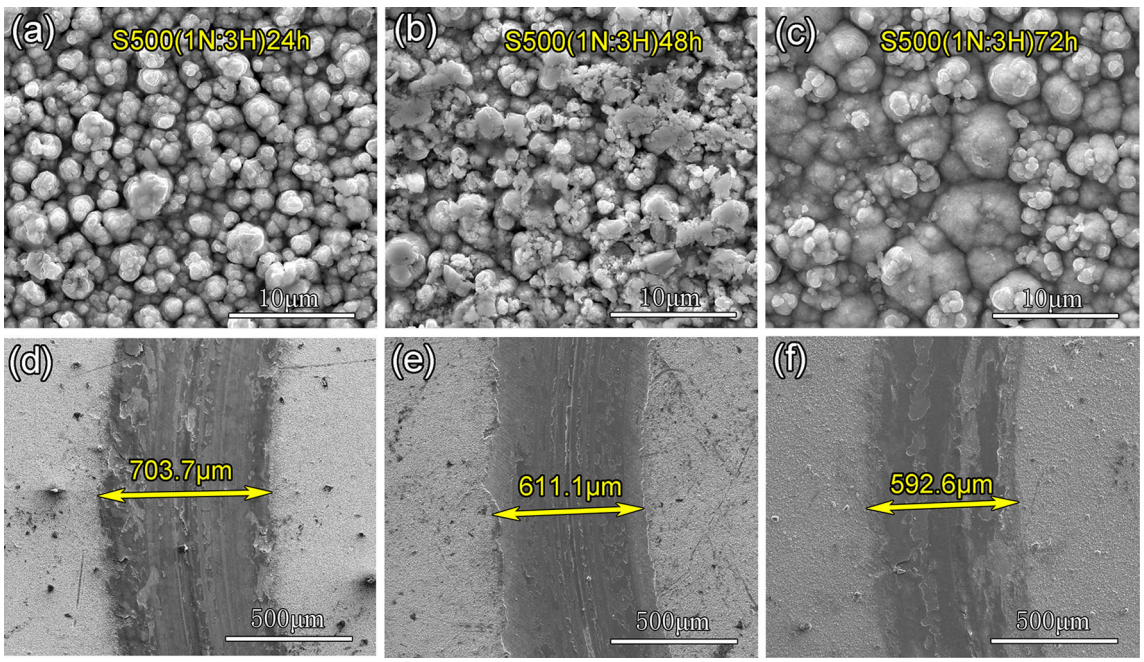

Fig. 7 Morphologies of nitrided surfaces and wear tracks of steel 38CrMoAl plasma nitrided at 500 °C for different time, **a** and **d** 24 h, **b** and **e** 48 h, **c**, **f** 72 h

reducing the plastic deformation during sliding. Thus, single phase γ′ is beneficial to tribological properties.

Figure 6 shows the frictional coefficients and wear rates of steel 38CrMoAl plasma nitrided at 500 °C for 24, 48 and 72 h. The specimen nitrided for 72 h with the strongest preferred orientation of (200)γ′ shows the lowest frictional coefficient and lowest wear rate. Figure 7 exhibits the surface morphologies and wear tracks for the steel 38CrMoAl plasma nitrided at 500 °C for different time. The nitrided surfaces shown in Fig. 7a–c are similarly characterized by particles distributed homogeneously. The 24 h and 48 h nitrided specimens are quite similar in particle sizes. However, for the 72 h nitrided specimen, a dramatic increase in the particle size is observed due to the phenomenon of Ostwald Ripening [23]. The wear tracks of specimens become narrower and shallower with the increase in the nitriding time. Therefore, the wear resistance is promoted with increasing preferred orientation of (200)γ′.

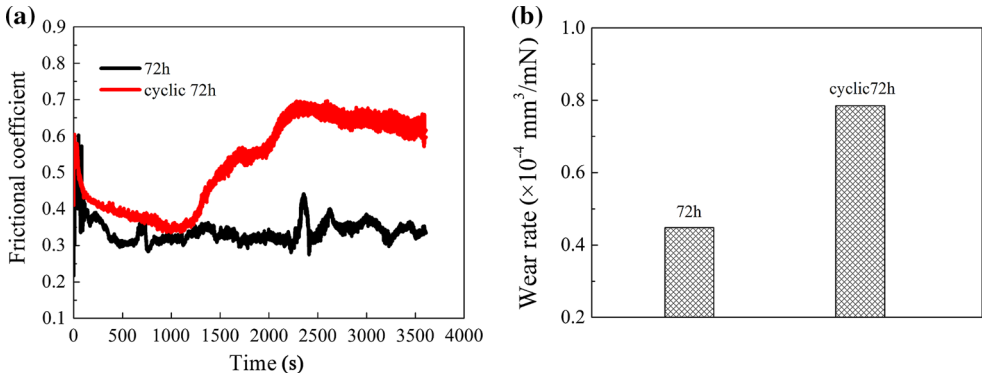

Fig. 8 Frictional coefficients **a** and wear rates **b** of steel 38CrMoAl plasma nitrided at 500 °C for 72 h and cyclic plasma nitrided between 420 and 500 °C for 72 h

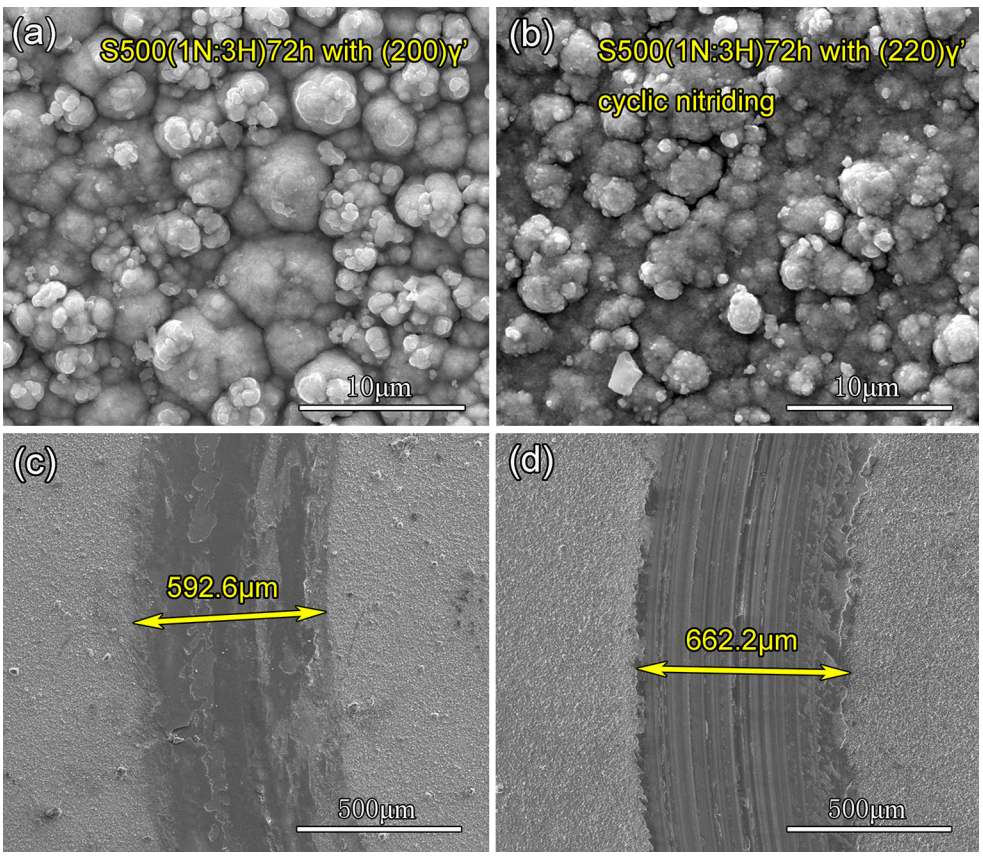

Fig. 9 **a** and **c** Morphologies of nitrided surface and wear track of steel 38CrMoAl plasma nitrided at 500 °C for 72 h, **b**, **d** morphologies of nitrided surface and wear track of steel 38CrMoAl cyclic nitrided between 420 and 500 °C for 72 h

The influences of preferred orientation of $(200)\gamma'$ and $(220)\gamma'$ on the wear properties of the steel 38CrMoAl are further characterized by the comparison between the conventional and cyclic plasma nitriding for 72 h. The frictional coefficients and wear rates for the specimens are shown in Fig. 8. The 72 h plasma nitrided specimen with preferred orientation of $(200)\gamma'$ exhibits much lower frictional coefficient and wear rate in comparison with the cyclic one. As discussed above, the transition between planes of $(1\bar{1}03)\varepsilon$ and $(220)\gamma'$ always is accompanied by distortion of lattice due to the relative larger misfit of interatomic distance (δ) of 2.67%. Such structure is detrimental to the tribological properties for the high internal stresses arising from the distortion of the lattice, which also can be verified by the worn morphologies observation in Fig. 9. The particle size for the cyclic 72 h nitrided surface is smaller than that for the 72 h nitrided one. The wear track for the cyclic 72 h nitrided specimen is much wider with parallel furrows and significant fragmentation due to the high internal stresses aroused by severe lattice distortion. The debris peeling off works as abrasion during sliding, resulting in typical abrasive wear and higher wear rate.

In a word, the preferred orientation of $(200)\gamma'$ has a positive significance in improving the wear properties of steels.

4 Conclusion

The crystallography texture of γ'-Fe_4N in compound layer and its influences on the tribological properties of nitrided steel 38CrMoAl are investigated in this work. The preferred orientation of $(200)\gamma'$ is produced under the nitriding condition of low temperature and low nitrogen containing atmosphere and increases with the nitriding time. The preferred orientation of $(220)\gamma'$ appears in the surface layer after 72 h cyclic nitriding. By first-principles method, such orientation relationships (ORs), $(0001)_\varepsilon//(110)_{\alpha'}$ and $[110]_\varepsilon//[111]_{\alpha'}$, $(111)_{\gamma'}//(0001)_\varepsilon$ and $[011]_{\gamma'}//[1\bar{2}10]_\varepsilon$, $(200)_{\gamma'}//(110)_{\alpha'}$ and $[011]_{\gamma'}//[111]_{\alpha'}$, as well as $(1\bar{1}03)_\varepsilon//(220)_{\gamma'}$ and $[0100]_\varepsilon//[1\bar{1}0]_{\gamma'}$ are established. The misfit of interatomic distance (δ), determining the reaction pathways and the preferred orientation, is calculated. Accordingly, two kinds of reaction pathways during nitriding, $\alpha'\rightarrow\varepsilon\rightarrow\gamma'$ or $\alpha'\rightarrow\gamma'$, are assumed. The preferred orientation of $(200)\gamma'$ usually results in lower frictional coefficient and wear rate in comparison with the preferred orientation of $(220)\gamma'$. $(111)\gamma'$ texture usually relates to the lower frictional coefficient but higher wear rate due to the slip system parallel to the sliding plane. In summary, the preferred orientation of $(200)\gamma'$ has a positive significance in improving the wear properties of nitrided steels.

Acknowledgements This work was financially supported by the National Natural Science Foundation of China (Grant Nos. 51371070 and 51601048).

References

[1] F. Bridier, P. Villechaise, J. Mendez, Acta Mater. **53**, 555 (2005)
[2] P. Villechaise, L. Sabatier, J.C. Girard, Mater. Sci. Eng. A **323**, 377 (2002)
[3] Z.N. Farhat, Wear **250**, 401 (2001)
[4] M. Mineur, P. Villechaise, J. Mendez, Mater. Sci. Eng. A **286**, 257 (2000)
[5] G. Bertolino, V. Doquet, M. Sauzay, Int. J. Fatigue **27**, 471 (2005)
[6] J.C. Stinville, P. Villechaise, C. Templier, J.P. Riviere, M. Drouet, Surf. Coat. Technol. **204**, 1947 (2010)
[7] P.E. Markovsky, Y.V. Matviychuk, V.I. Bondarchuk, Mater. Sci. Eng. A **559**, 782 (2013)
[8] H.Y. Yang, J. Li, P. Yang, Acta Metall. **28**, 289 (2015)
[9] C.X. He, F.Y. Yang, G. Ma, X. Chen, L. Meng, Acta Metall. **29**, 554 (2016)
[10] Z.S. Yu, J.X. Zhang, H.Z. Wang, R.C. Zhou, Y. Yuan, Acta Metall. **30**, 156 (2016)
[11] C. Zhang, L.W. Zhang, W.F. Shen, Y.N. Xia, Y.T. Yan, Acta Metall. **30**, 79 (2016)
[12] J.C. Stinville, P. Villechaise, C. Templier, J.P. Riviere, M. Drouet, Acta Mater. **58**, 2814 (2010)
[13] S.H. Kim, S.H. Jeong, T.H. Kim, J.H. Choi, S.H. Cho, B.S. Kim, S.W. Lee, Ceram. Int. **43**, 9200 (2017)
[14] Y.F. Xu, Y.B. Peng, K.D. Dearn, T. You, J. Geng, X.G. Hu, Surf. Coat. Technol. **313**, 391 (2017)
[15] G. Abrasonis, J.P. Riviere, C. Templier, A. Declémy, L. Pranevicius, X. Milhet, J. Appl. Phys. **97**, 1 (2005)
[16] B.R. Zhang, S.Q. Wang, D.S. Sun, F.Z. Li, Z.M. Jiang, J. Shandong Polytech. Uni. **3**, 60 (1986)
[17] M.F. Yan, Y.Q. Wu, R.L. Liu, Appl. Surf. Sci. **255**, 8902 (2009)
[18] Y.Q. Wu, M.F. Yan, Vacuum **86**, 119 (2011)
[19] K. Shetty, S. Kumar, P.R. Rao, Surf. Coat. Technol. **203**, 1530 (2009)
[20] M. Shafiei, A.T. Alpas, Wear **265**, 429 (2008)
[21] S.K. Kim, J.S. Yoo, J.M. Priest, M.P. Fewell, Surf. Coat. Technol. **163–164**, 380 (2003)
[22] Z.Q. Liu, Z.K. Hei, D.X. Li, J. Mater. Res. **17**, 2621 (2002)
[23] L. Ratke, P.W. Voorhees, *Growth and Coarsening Ostwald Ripening in Material Processing* (Springer, Berlin, 2002)